

Optimal automated design of EMI filter for mitigating conducted electromagnetic disturbance in photovoltaic DC-DC converters

Optymalny zautomatyzowany projekt filtra EMI w celu łagodzenia przewodzonych zakłóceń elektromagnetycznych w fotowoltaicznych przetwornikach DC-DC

Abstract. This paper focuses on optimizing the electromagnetic interference (EMI) filter design of DC-DC boost converters for photovoltaic (PV) systems. A comprehensive computer-aided procedure is presented, which integrates the parasitic elements of the EMI filter, to achieve precise automated design with volume reduction. This procedure is guided by strict rules and precise measurements, relying on comprehensive databases sourced from commercial data sheets related to passive components. It also takes into account the parasitic capacitance of boost converters. Experimental validations of the proposed algorithm are presented, using the EN 55022 Class B standard as a reference to rigorously assess the performance of the proposed filter circuit for mitigating conducted electromagnetic disturbances in DC-DC converter.

Streszczenie. Niniejszy artykuł koncentruje się na optymalizacji projektu filtra zakłóceń elektromagnetycznych (EMI) przetwornic podwyższających napięcie DC-DC dla systemów fotowoltaicznych (PV). Przedstawiono kompleksową procedurę wspomaganą komputerowo, która integruje elementy pasożytnicze filtra EMI, aby osiągnąć precyzyjny zautomatyzowany projekt ze zmniejszeniem objętości. Ta procedura jest prowadzona według ścisłych zasad i precyzyjnych pomiarów, opierając się na kompleksowych bazach danych pochodzących z komercyjnych arkuszy danych dotyczących elementów pasywnych. Bierze również pod uwagę pojemność pasożytniczą przetwornic podwyższających napięcie. Przedstawiono eksperymentalne walidacje proponowanego algorytmu, wykorzystując normę EN 55022 klasy B jako odniesienie do rygorystycznej oceny wydajności proponowanego obwodu filtra w celu łagodzenia przewodzonych zakłóceń elektromagnetycznych w przetwornicy DC-DC.

Keywords: EMI filter, photovoltaic DC-DC converter, parasitic elements, automated design

Słowa kluczowe: Filtr EMI, przetwornica DC-DC fotowoltaiczna, elementy pasożytnicze, projektowanie automatyczne

Introduction

In recent years, the global demand for renewable energy has surged significantly due to rapid population growth and the accelerated pace of industrial development. Photovoltaic (PV) energy stands out as one of the most crucial green energy sources, because of its sustained sustainability and wide availability in the natural world. The photovoltaic system necessitates seamless integration between electronic devices and control techniques to achieve maximum power transfer during the energy conversion process, ensuring highly efficient output [1]. A crucial component of a photovoltaic system connected to a DC network is a converter, which adjusts the voltage and/or current level for the load or end user. This converter increases adjusts the electrical voltage to the necessary level for operating the equipment or device [2, 3].

During operation of the DC-DC converter, rapid variations in voltage (dv/dt) and current (di/dt) can lead to the generation of electromagnetic interference (EMI)[4-6]. EMI encompasses both conducted and radiated interference, which are emitted from the "source" equipment into the surrounding environment. This interference adversely affects the normal operation of other equipment, referred to as "victim" devices, within the same environment. The generated noise propagates in two distinct modes: common mode (CM) and differential mode (DM) [7, 8]. Therefore, proposing EMI attenuation solutions into practice is crucial to guaranteeing the system's overall electromagnetic compatibility (EMC) and dependability, including the power electronic converter [2,8]. In this context, numerous solutions have been proposed in the literature for noise mitigation. The first solution often employed is the use of passive EMI filters[9,10]. These filters significantly reduce noise; however, their size and the presence of parasitic elements limit their effectiveness in applications with strict volume constraints and their efficiency across the entire attenuation range [11,12]. To minimize the impact of parasitic elements in passive EMI filters, several research papers propose methods to reduce

the propagation paths. Among these strategies is determining the optimal position of the elements [12,13], aiming to reduce the magnetic coupling between filter components and achieve maximum attenuation. Enhancing flux distribution over the core cross-section at high frequencies may also be achieved by changing the material of the choke coils on the loop cores, thereby improving the overall performance of the EMI filter [14]. Alternatively, an equivalent circuit model can be adopted for the EMI filter, which includes the self-parasitics of each individual component. In this model, the inductor is represented by an equivalent parallel resistance (EPR) and an equivalent parallel capacitance (EPC), while the capacitor is characterized by an equivalent series resistance (ESR) and an equivalent series inductance (ESL)[15,16]. This method depends on measurement and repetition to ensure the elements achieve the best attenuation. Accordingly, some references have suggested automated design methods based on high-frequency models to improve the filter's performance and reduce its size [11] [16-18].

This article addresses EMI generated by DC-DC boost converters used in photovoltaic systems. Photovoltaic systems are intended to use this converter. Therefore, only a passive EMI filter, comprising passive components, is used to provide filtering for the proposed DC-DC converter [2]. Emissions in CM and DM can be measured and separated using a Line Impedance Stabilization Network (LISN) and a noise separator [19]. Numerous studies have been conducted on noise suppression in PV systems [20-22]. Studies [22,23] in EMI modeling have made significant progress. Still, not enough research has been done on the system's high-frequency modeling. Furthermore, there are still a number of difficulties in the design of conventional EMI filters. These include the need to optimize their size, account for parasitic elements, and undergo repeated testing procedures.

This paper aims to develop an automated optimization tool for designing EMI filters in DC-DC boost converters used in PV systems. The process entails evaluating the

parasitic capacitance of boost converters and choosing filter characteristics for passive components from commercial data sheets. Additionally, it considers optimizing the EMI filter volume. The test setup allows for experimental evaluation of the automated design process by comparing the noise levels against the EN55022 Class B standard.

The equipment under test is a DC-DC boost converter used on the DC side of the PV system and Conducted EMI transmission, as shown in Figure 1, with its characteristics detailed in Table 1. Consequently, it is crucial to follow solar system rules, particularly the EN55022 Class B standard, which specifies electromagnetic interference measurement settings and limit values for equipment emissions and susceptibility.

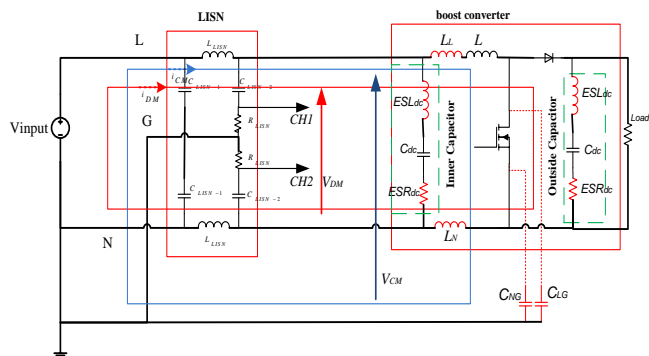


Fig.1. Conducted EMI transmission in DC-DC converter with elevated high-frequency parasitic parameters

Table 1. The parameters of DC-DC converter with parasitic parameters

Parameter	Value
Switching frequency F	10 kHz
Duty cycle D	0.7
Input voltage V_{input}	12 V
Load R	10Ω
Bobbin L	20mH
Parasitic capacitors of converter C_{NG} and C_{LG}	145.08pF and 204.88pF
Parasitic inductances of converter L_N and L_L	71.49nH and 75.78nH
Equivalent circuit model DC inner and outside capacitors ESL_{dc} , ESR_{dc} and C_{dc}	158.31nH, 200mΩ and 100μF

The proposed optimized design of EMI filter

The proposed design process implements a rule-based algorithm, taking into account the specific requirements of the filter application. This includes the noise circuits, relevant constraints, parasitic elements in the filter design, and databases of commercially available components for configuring EMI filters. The flowchart of the design method is illustrated in Fig. 2.

First, the designer must compile the input data which depends on the measurement.

Three comprehensive databases cataloging available market devices have been developed. The first database focuses on magnetic cores and includes essential information. Additionally, a second database of film capacitors has been created.

Finally, a third database focusing on wiring was created, the winding angle ($\sigma_{winding}$) resulting from the winding process. We assume that the winding angle is 145° and the diameter of the copper conductor (D_{wire}) is 1.5 mm.

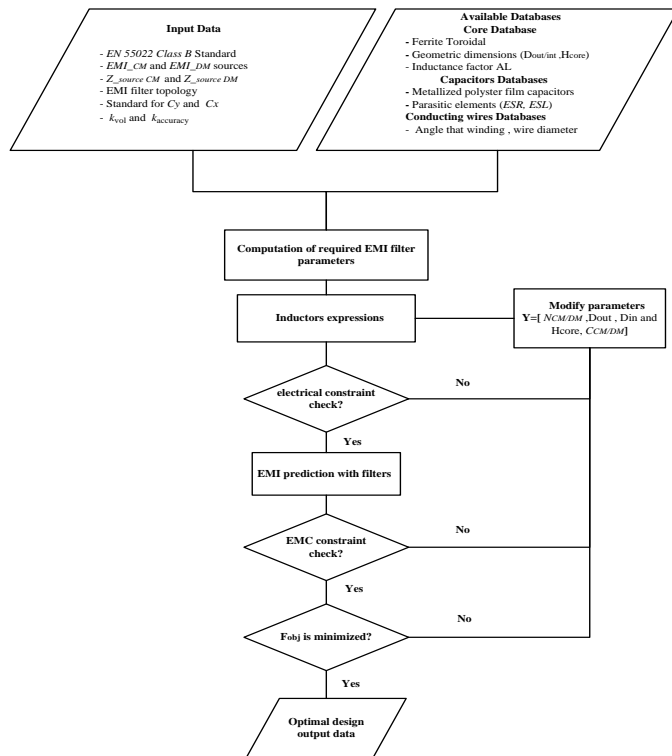


Fig. 2. The flowchart for the proposed EMI filter design

Computation of required EMI filter parameters

In the initial step, the algorithm pinpoints critical points between the peaks in the EMI spectra that correspond to the frequencies of the CM/DM components targeted for attenuation ($f_{CM_att_h}$ and $f_{DM_att_h}$). Subsequently, it calculates the necessary attenuations for CM and DM noise [9,11], as defined by the following equations:

$$(1) Att_{req_CM/DM} = EMI_{h_CM/DM} - EMI_{Stand} + Marg$$

where: EMI_{h_CM} and EMI_{h_DM} – amplitudes CM/DM of frequency spectrum components targeted for attenuation, EMI_{Stand} – maximum amplitude, $Marg$ – safety margin.

The cutoff frequency ($f_{0_CM/DM}$) is determined, considering that the attenuation of the filter commences at this frequency and escalates with $Att_{inhr_CM/DM}$, which represents the filter's inherent attenuation closely tied to its topology [8]. Consequently, the corner frequency can be evaluated as follows:

$$(2) Att_{req_CM/DM} = Att_{inhr_CM/DM} \log \left(\frac{f_{CM/DM_att_h}}{f_{0_CM/DM}} \right)$$

thus obtaining:

$$(3) L_{req_CM/DM} = \left(\frac{1}{C_{CM/DM} (2\pi \cdot f_{0_CM/DM})^2} \right)$$

Expressions and Design Considerations for Inductors

The initial step involves selecting a toroidal core from the database and determining the wire diameter (D_{wire}) based on the peak operating current specified by the designer, as well as the winding angle ($\sigma_{winding}$) [17]. Subsequently, the maximum number of achievable turns (N_{max}) is calculated using the following formula:

$$(3) N_{max} = \left(\frac{2 \cdot \sigma_{winding} \cdot \pi}{360} \right) \left[\frac{D_{in} - D_{wire}}{D_{wire}} \right]$$

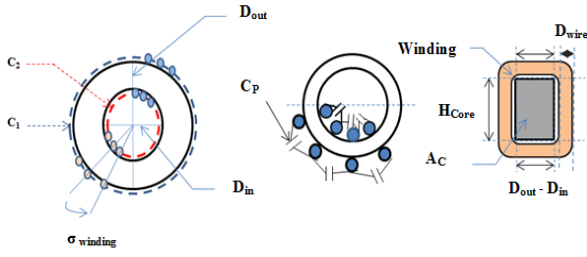


Fig. 3. Geometric parameters of the toroidal core.

After calculating the number of turns $N_{CM/DM}$ needed the computed inductance value is a function of the geometric parameters of the toroidal core is illustrated in Fig. 3 [3,11], as described by the following equation:

$$(4) L_{CM/DM} = \left(\frac{N_{CM/DM}^2 \cdot \mu_0 \mu_r}{\pi} \right) \left[\frac{D_{out} - D_{in}}{D_{out} + D_{in}} \right]$$

where: μ_0 and μ_r – vacuum and relative core permeability respectively.

Additionally, the capacitance between the windings (EPC) of the inductor is a key factor that primarily induces resonances at high frequencies ($f_{r_L_CM/DM}$), as calculated in Equation (5).

$$(5) f_{r_L_CM/DM} = \frac{1}{2\pi \sqrt{L_{CM/DM} \cdot EPC_{CM/DM}}}$$

Accurately estimating this capacitance is crucial [12,24]. The calculation is performed using the following formula:

$$(6) EPC_{CM/DM} = 1.366 \cdot \epsilon_0 \pi \cdot L_{turn} \left(\frac{\epsilon_r \theta}{\ln[D_{out}/D_{in}]} + \cot\left(\frac{\theta}{2}\right) - 1 \right)$$

Where:

$$\theta = \arccos\left(1 - \frac{\ln(D_{out}/D_{in})}{\epsilon_r}\right)$$

ϵ_r – permittivity of the dielectric, ϵ_0 – vacuum permittivity and L_{turn} – length of a turn.

For toroidal inductors, the volume ($Vol_{LCM/DM}$) is determined by the following equation:

$$(7) Vol_{LCM/DM} = ((D_{out}/2) + D_{wire})^2 \cdot (H_{core} + 2 \cdot D_{wire})$$

EMI prediction with filter

The LTSpice tool is utilized to predict the emissions generated by the proposed converter, as shown in Fig. 4. To ensure that the simulation results closely align with the experimental outcomes, parasitic elements of both the CM and DM EMI filter and the converter are included in the model [15,21]. Additionally, a LISN model is inserted between the converter and the power source. This setup prevents EMI from passing between them, stabilizes the power supply impedance, and measures the conducted emissions of the DC-DC boost converter [19]. For the design process to work, a link must be made between MATLAB and LTSpice to automatically adjust optimization parameters and initiate simulations.

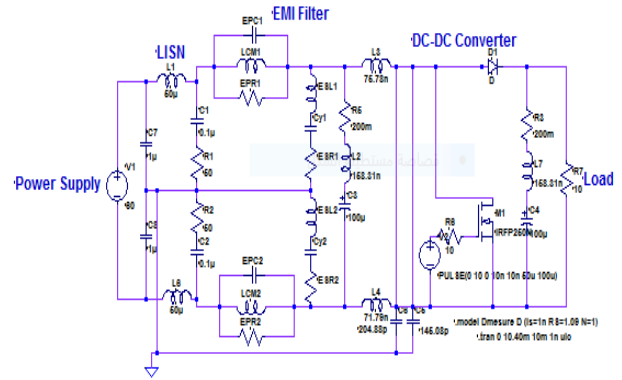


Fig. 4. DC-DC Converter simulation circuit in LTSpice.

Optimization algorithms

The filter design process involves considering multiple constraints [18], including the EMC constraint in Equation (8) and the electrical constraint in Equation (9).

$$(8) EMI_{filter_CM/DM}(Y, Freq) \leq EMI_{stand}(Freq)$$

where: $EMI_{filter_CM/DM}$ – interference CM and DM with the optimization parameters (Y) for each processed frequency ($Freq$).

$$(9) N_{CM/DM} \leq N_{max}/2$$

The objective function to be minimized combines volume (Vol_{filter}) and EMI standard deviation (SD) with the filter, as detailed in Equation (10). MATLAB's "fgoalattain" is used as a nonlinear programming solver to find the minimum of this objective function. After several iterations, the optimization algorithm converges to an optimal selection of $Y = [N_{CM/DM}, D_{out}, D_{in}, H_{core}, C_x, C_y, ESR, ESL]$ related to the filter components.

$$(10) F_{obj} = \min(k_{vol} \cdot Vol_{filter} + k_{accuracy} \cdot SD(Y, Freq))$$

where: k_{vol} and $k_{accuracy}$ – Coefficients specified for volume and EMI filter accuracy.

$$Vol_{filter} = \sum_{i=1}^n Vol_{L_{CM/DM_i}} + \sum_{i=1}^n Vol_{C_{CM/DM_i}}$$

$$SD(Y, Freq) = \sqrt{\frac{\sum_{i=1}^N |EMI_{filterCM/DM}(Y, Freq) - EMI_{stand}(Freq)|^2}{N}}$$

N – number of frequencies evaluated

Experimental results

Provide the design process has been rigorously validated through experimental investigations conducted on a specially designed test bench. Fig.5 illustrates the photovoltaic DC-DC boost converter under examination, along with the DC generator, load frequency generator (LFG), oscilloscope, and LISN.

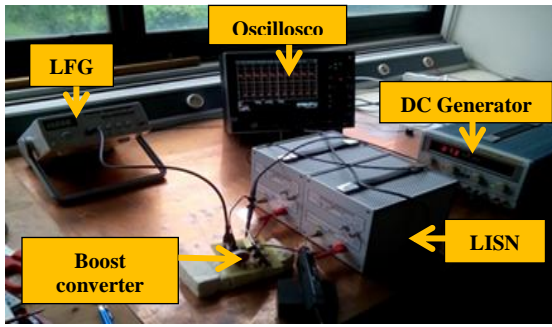


Fig. 5. Experiment setup.

In Figures 6 and 7, the input data used for the automated design process are reported.

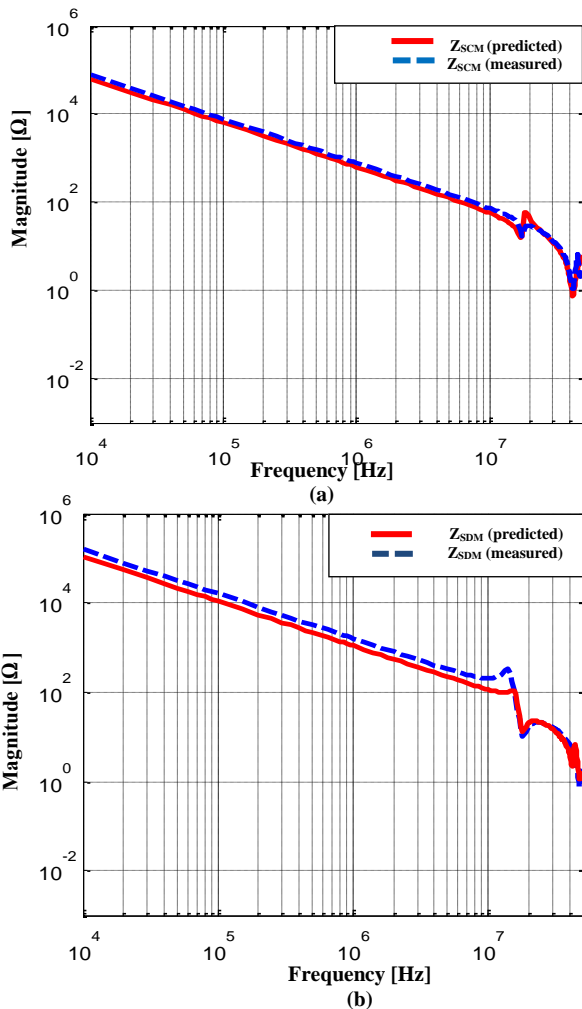


Fig. 6. Noise source impedance predicted by the LTSPICE model and measured on the (a) CM and (b) DM.

The results illustrated in Figure 6 clearly demonstrate that the impedances Z_{SCM} and Z_{SDM} exhibit capacitive behavior within the frequency range of 10 kHz to approximately 10 MHz. This behavior is predominantly influenced by the parasitic capacitances between the transformer PCB and the copper plane.

As shown in Figures 7(a) and 7(b), the conducted emission levels of EMI CM and EMI DM without filter exceed the EN55022 Class B thresholds—55 dB μ V for the 0.5 MHz to 5 MHz range and 40 dB μ V for the 5 MHz to 30 MHz range—across most of the frequency spectrum. To comply with EMC standards, the designed EMI filter must provide greater attenuation than these thresholds.

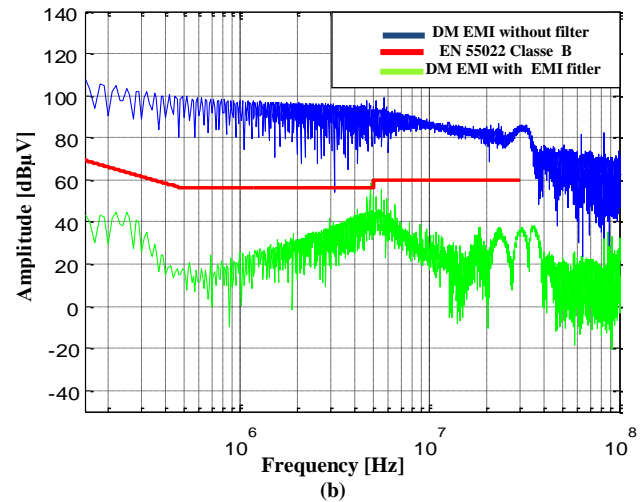
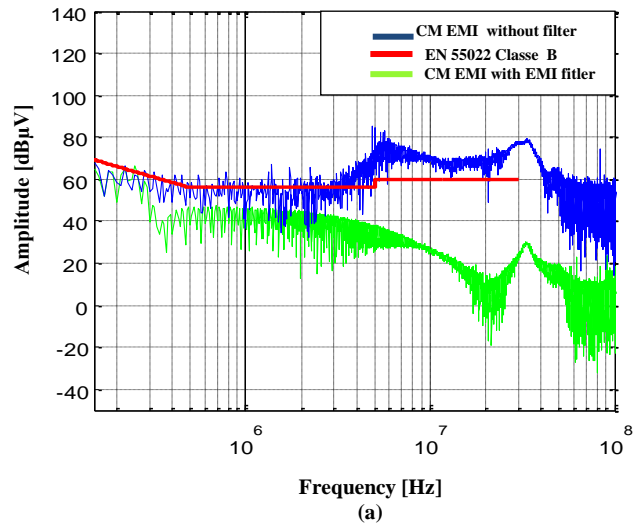


Fig. 7. Measured EMI noise without/with EMI filter compared with the EN 55022 Class B standard.(a) CM EMI filter, (b) DM EMI filter.

The results obtained from the optimization design, including the filter element values, calculated parasitic elements, and volume, are presented in Tables 2 and 3.

Table 2. Output data for CM inductor and DM inductor

Characteristics	CM inductor	DM inductor
Inductance factor AL	100 nH	1000 nH
Inductance value L	25.6 μ H	32.4 μ H
Number of turns N	16 turns	18 turns
Inductor core dimensions Dout \times Din \times Hcore	34 \times 20 \times 12.5 mm \times mm \times mm	58.3 \times 40.8 \times 40.2 mm \times mm \times mm
Volume	5.3 cm ³	21.49 cm ³
Core materials	Ferrite K1 toroid	Ferrite K10 toroid
Model	B64290L0048X001	B64290A0042X010
Equivalent parallel resistance EPR	1.85 k Ω	11.5 k Ω
Equivalent parallel capacitance EPC	2.476 pF	54.34 pF
Diameter of wire D_{wire}	1.5 mm	1.5 mm
Winding angle $\sigma_{winding}$	145 $^\circ$	145 $^\circ$

Table 3. Output data for C_x and C_y

Characteristics	C_x and C_y
Capacitor value C	2.2 μ F
Dimensions w \times h \times l	7 \times 16 \times 17.5 mm \times mm \times mm
Volume	1.915 cm ³
Materials	Polyester film
Model	MKT468
Equivalent series resistance ESR	16 m Ω
Equivalent series inductance ESL	20.49 nH

The total volume of the EMI filter is 34.45 cm³, as detailed in Tables 6 and 7. The DM filter occupies 25.32 cm³, which constitutes 73.5% of the total volume.

Figures 8 respectively present the impedance curve of the optimized filter elements and the emission levels with the filter.

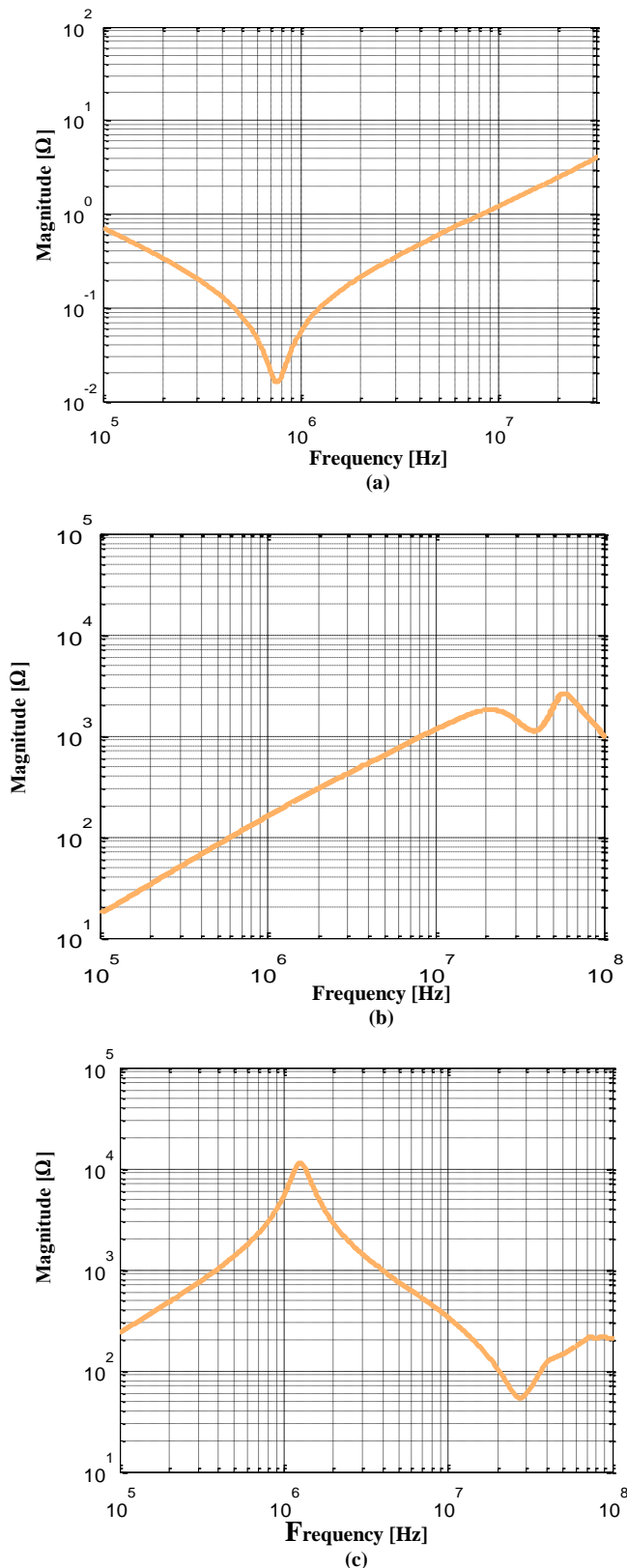


Fig. 8. The impedance curve of the (a) CM/DM capacitor, (b) CM inductor and (c) DM inductor.

As shown in Figure 8(a) and (b), the self-resonant frequency of the CM capacitor is 0.7531 MHz, significantly higher than 0.320 MHz. This allows the CM capacitor to effectively attenuate CM noise. Additionally, the self-resonant frequency of the CM inductor is approximately 22.05 MHz, ensuring it provides the necessary impedance at other frequencies and maintains the performance of the CM filter.

Figure 8(c) depicts the impedance response of the DM inductor, with its self-resonant frequency at 1.269 MHz, delivering sufficient impedance to satisfy the necessary attenuation requirements.

In Figure 7(a) and (b), it is evident that the conductive emission levels of the EMI CM and EMI DM with the filter are sufficiently attenuated, staying well below the limits set by the EN 55022 Class B standard. However, there are exceptions at 250 kHz for CM and 4.5 MHz for DM, where the levels exceed the limits by a margin of 5 dB. These deviations are primarily attributed to modeling inaccuracies in the filter and variations in the power cable impedance. Despite these anomalies, the overall emission profile demonstrates excellent conformity and performance.

In Table.4, we have compared the performances of our work with others in literature. The numerical comparison in term of standard deviation (SD) value of EMI illustrates the efficiency of our work.

Table 4. A comparative study between the design of an EMI filter and other works

Reference	Design Methods	SD _{CM} [dBuV]	SD _{DM} [dBuV]
Ref [3]	Optimizing for reduced electrical losses.	42.44	/
Ref [10]	Design with measurement to confirm attenuation	20.84	/
Ref [11]	Automated design based on databases constructed	25.13	26.39
Ref [19]	Automatic design and optimization for filter volume.	27.23	/
Ref [20]	Automated design utilizing suitable databases	25.9	/
Ref [24]	Optimizing and conducting stabilization analysis	28	/
Our Method	Automated design and optimization that integrates parasitic elements.	19.1	22.52

Conclusion

The objective of this study is to provide high-performance EMI filters with the least amount of space by proposing an automated design approach especially targeting adapters in DC-DC boost converters used in PV systems. The procedure utilizes a carefully crafted rule-based algorithm within the Matlab environment, which seamlessly interfaces with the LT-Spice environment. It leverages databases of magnetic cores, capacitors, and conductive wires selected from commercially available options to ensure application suitability. The design takes into account inputs such as source impedances, noise measurements specific to DC-DC boost converters, and EMI standards that define the maximum allowable noise levels. Experimental validation of the suggested process

shows that it is a successful method for reducing conducted emissions.

Authors: Feteah Beggat, Laboratory of Instrumentation (LINS), Faculty of Electrical Engineering, University of Science and Technology Houari Boumediene (USTHB), BP 32 Bab Ezzouar, 16111, Algiers, Algeria; Email: fbeggat@usthb.dz; Prof.

Farid Bouchafaa, University of Science and Technology Houari Boumediene (USTHB), BP 32 Bab Ezzouar, 16111, Algiers, Algeria; Email: fbouchafa@usthb.dz; Dr Abdelhai Lati, University Kasdi Merbah Ouargla (UKMO), BP 511, 30000, Ouargla, Algeria; Email: lati.abdelhai@univ-ouargla.dz.

REFERENCES

- [1] D. Penciu, S. ANDREICA, R. GLIGA, C. MUNTEANU, M. PURCAR, and Ș. ARDELEANU, "Assessment of Electromagnetic Interferences Produced by a Photovoltaic On-Grid System," in 2023 10th International Conference on Modern Power Systems (MPS), 2023, pp. 1-4.
- [2] C. Jettanasen and C. Pothisarn, "Performance and electromagnetic interference mitigation of DC-DC converter connected to photovoltaic panel," *Int. J. of Smart Grid and Clean Energy*, vol. 8, pp. 806-812, 2019.
- [3] A. Ouhammam, H. Mahmoudi, Y. El Hachimi, and A. Daghour, "Simulation and optimization of EMI filter of conducted emission for high voltage gain DC-DC converter," *Simulation*, vol. 15, 2024.
- [4] M. T. Nooshabadi, J.-L. Schanen, H. Iman-Eini, and L. G. A. Rodrigues, "Optimization of EMI Filters of Multi-Level Flying Capacitor Boost Converter," *IEEE Transactions on Industry Applications*, 2024.
- [5] E. Şehirli, "Examining the Design of Different Types of DM EMI Filters and Their Effect on EMI Noise and Control Characteristics for Cuk DC-DC Converter," *International Transactions on Electrical Energy Systems*, vol. 2023, p. 7101065, 2023.
- [6] I. Grobler and M. N. Gitau, "Modelling and measurement of high-frequency conducted electromagnetic interference in DC-DC converters," *IET Science, Measurement & Technology*, vol. 11, pp. 495-503, 2017.
- [7] X. Ruan, L. Xie, Q. Ji, and X. Yuan, "Measurement of Conducted Electro-magnetic Interference (EMI) and Design of EMI Filter," in *Conducted Electromagnetic Interference in Power Converters: Modeling, Prediction and Reduction*, ed: Springer, 2024, pp. 25-38.
- [8] S. Takahashi, K. Wada, H. Ayano, S. Ogasawara, and T. Shimizu, "Review of modeling and suppression techniques for electromagnetic interference in power conversion systems," *IEEJ Journal of Industry Applications*, vol. 11, pp. 7-19, 2022.
- [9] D.-T. Do and H. Hirsch, "EMI filter performance of transformerless topology for photovoltaic applications," in 2020 International Symposium on Electromagnetic Compatibility-EMC EUROPE, 2020, pp. 1-6.
- [10] H. Hizarci, U. Pekperlak, and U. Arifoglu, "Conducted emission suppression using an EMI filter for grid-tied three-phase/level T-type solar inverter," *IEEE Access*, vol. 9, pp. 67417-67431, 2021.
- [11] G. Giglia, G. Ala, M. C. Di Piazza, G. C. Giaconia, M. Luna, G. Vitale, et al., "Automatic EMI filter design for power electronic converters oriented to high power density," *Electronics*, vol. 7, p. 9, 2018.
- [12] N. Jia, L. Xue, and H. Cui, "Mitigating EMI Noise in Propagation Paths: Review of Parasitic and Coupling Effects in Power Electronic Packages, Filters, and Systems," *IEEE Open Journal of Power Electronics*, 2024.
- [13] M. Ali, J. Friebe, and A. Mertens, "Design and Optimization of Input and Output EMI Filters under the Influence of Parasitic Couplings," in 2021 23rd European Conference on Power Electronics and Applications (EPE'21 ECCE Europe), 2021, pp. 1-10.
- [14] P. Gonzalez-Vizuet, J. Bernal-Mendez, M. J. Freire, and M. A. Martin-Prats, "Improving performance of compact EMI filters by using metallic and ferrite sheets," *IEEE Transactions on Power Electronics*, vol. 36, pp. 9057-9068, 2021.
- [15] R. He, Y. Xu, S. Walunj, S. Yong, V. Khilkevich, D. Pommerenke, et al., "Modeling strategy for EMI filters," *IEEE Transactions on Electromagnetic Compatibility*, vol. 62, pp. 1572-1581, 2020.
- [16] S. Negri, G. Spadacini, F. Grassi, and S. A. Pignari, "Black-box modeling of EMI filters for frequency and time-domain simulations," *IEEE Transactions on Electromagnetic Compatibility*, vol. 64, pp. 119-128, 2021.
- [17] D. Zhang, T. Fan, P. Ning, and X. Wen, "An automatic EMI filter design methodology for electric vehicle application," in 2017 IEEE Energy Conversion Congress and Exposition (ECCE), 2017, pp. 4497-4503.
- [18] G. Ala, G. Giaconia, G. Giglia, M. Di Piazza, M. Luna, G. Vitale, et al., "Computer aided optimal design of high power density EMI filters," in 2016 IEEE 16th International Conference on Environment and Electrical Engineering (EEEEIC), 2016, pp. 1-6.
- [19] Y. Sugiura, K. Wada, and S. Takahashi, "Measurement of DC-side Electromagnetic Noise inside Photovoltaic Power Converters," in 2021 IEEE International Future Energy Electronics Conference (IFEEEC), 2021, pp. 1-5.
- [20] T. A. W. Wijanarko, Y. Yudhistira, D. Mandaris, H. W. Nugroho, Y. Yoppy, A. N. Bakti, et al., "Characterization of conducted emissions at DC line of off-grid PV systems," in AIP Conference Proceedings, 2024.
- [21] J. Zhang, W. Chen, B. Zhang, X. Song, and H. Huang, "Optimal design of EMI filters for PV system based on parasitic parameter and stability analysis," in 2015 9th International Conference on Power Electronics and ECCE Asia (ICPE-ECCE Asia), 2015, pp. 2744-2751.
- [22] W. Qiu, L. Zhang, H. Yin, L. C. Markel, D. Liao, B. W. McConnell, et al., "Modeling, testing, and mitigation of electromagnetic pulse on PV systems," *Solar Energy*, vol. 264, p. 112010, 2023.
- [23] M. T. Nooshabadi, J.-L. Schanen, S. Farhangi, and H. Iman-Eini, "Frequency Model for EMI Study of Three-Phase Grid Connected Photovoltaic Inverter on Both DC and AC Sides," in 2023 IEEE Applied Power Electronics Conference and Exposition (APEC), 2023, pp. 620-625.
- [24] S. W. Pasko, M. K. Kazimierczuk, and B. Grzesik, "Self-capacitance of coupled toroidal inductors for EMI filters," *IEEE Transactions on Electromagnetic Compatibility*, vol. 57, pp. 216-223, 2015.